Colloids and Surfaces B: Biointerfaces 97 (2012) 150–154

Contents lists available at SciVerse ScienceDirect

Colloids and Surfaces B: Biointerfaces

journal homepage: www.elsevier.com/locate/colsurfb

Highly sensitive electrochemical impedance sensing of PEP gene based on integrated Au–Pt alloy nanoparticles and polytyramine

Tao Yang, Na Zhou, Qianhe Li, Qian Guan, Wei Zhang, Kui Jiao*

Shandong Provincial Key Laboratory of Biochemical Analysis, College of Chemistry and Molecular Engineering, Qingdao University of Science and Technology, Qingdao 266042, PR China

ARTICLE INFO

Article history:
Received 8 September 2011
Received in revised form 28 March 2012
Accepted 5 April 2012
Available online 12 April 2012

Keywords:
Au–Pt alloy nanoparticles
Polytyramine
DNA biosensor
Electrochemical impedance spectroscopy
PEP gene

ABSTRACT

Fabrication of an electrochemical impedimetric DNA biosensor based on the integration of Au–Pt alloy nanoparticles (Au–Pt_{NPs}) and electropolymerized polytyramine (Pty) film for the detection of phosphoenolpyruvate carboxylase (PEP) gene is described in this article, where Pty films acted as an ideal combination platform for Au–Pt_{NPs} via electrostatic adsorption. The electrochemical properties of the Au–Pt_{NPs}/Pty, the characteristics of the immobilization and hybridization of DNA were investigated by cyclic voltammetry, differential pulse voltammetry and electrochemical impedance spectroscopy (EIS), respectively. Primary study indicated that Au–Pt_{NPs}/Pty had a synergistic effect on the electrochemical signal of $[Fe(CN)_6]^{3-/4-}$, which served as the classic redox probe in the most electrochemical impedimetric sensors. DNA sequence-specific of PEP transgene existed in some transgenic crops was detected by this EIS protocol. The dynamic detection range of this DNA electrochemical biosensor to the DNA target sequence was from 1.0×10^{-12} M to 1.0×10^{-7} M. The detection limit was measured to be 3.6×10^{-13} M. The DNA biosensor also had good selectivity, stability and reproducibility.

1. Introduction

Up to now, the transgenic plants have received considerable attention all over the world. The transgenic plants play a very important role in reducing the environmental footprint of agriculture and greenhouse gases, contributing to the alleviation of poverty and hunger, and mitigating climate change [1]. At the same time, the security of the transgenic plants for the consumer and environment has also cause people's attention [2]. Therefore, the detection of the transgenic plant is of great significance. DNA electrochemical biosensor, which is widely used owing to its high sensitivity, simplicity and low cost compared with other analytical techniques [3–5], has become one of the most important methods for the detection of transgenic plant products [6–8].

Bimetallic alloy nanoparticles, such as Au–Pt_{NPs} and Au–Ag_{NPs} [9–11] often exhibit better catalytic properties than do their monometallic counterparts. Thus, they have attracted considerable interest in the field of catalysis and sensors. For example, Au–Pt alloy nanoparticles have widely applied in selective oxidation, dehydrogenation catalysis, electrocatalysts, and selective sensors [12–14]. Qian et al. [15] fabricated Au–Pt bimetallic flower nanostructures on a polyamidoamine dendrimers-modified surface by electrodeposition. The bimetallic nanoflowers-modified electrode exhibited significant electrocatalytic activities toward oxygen reduction. Lang et al. [16] reported that bimetallic dendrimer-stabilized nanoparticles were used to prepare supported Pt–Au catalysts within the bulk miscibility gap for the binary system.

Nowadays electropolymerization of conducting polymers, such as polypyrrole, polyaniline, and polythiophene, has been thoroughly investigated for the fabrication of biosensors, due to their high conductivity and stability both in air and in aqueous solution [17–19]. Among kinds of polymers, polytyramine (Pty) which presents one primary aliphatic amine per tyramine moiety has received attention due to its very high surface concentration of reactive sites for immobilization of biomolecules [20–24]. For instance, Mantzila et al. [24] described a faradic impedimetric immunosensor based on electropolymerized Pty films. The proposed immunosensor was successfully used for the detection of *Salmonella typhimurium* in experimentally inoculated milk samples.

Composite materials consisting of polymer and metal nanoparticles have been the subject of much interest recently. Deposition of metal micro-nanostructures on polymer matrices may combine interesting properties of both components. Polymeric films could provide unique electrochemical properties and improve the stability of the metal nanoparticles [25–27].

In this work, the Pty film was initially electropolymerized using cyclic voltammetry (CV) to introduce amino groups on the surface of a glassy carbon electrode. The Pty film was ideal for the nucleation and crystal growth of Au–Pt_{NPs} via electrodeposition.

* Corresponding author. Tel.: +86 532 84855977; fax: +86 532 84023927.
E-mail address: kjiao@qust.edu.cn (K. Jiao).

0927-7765/$ – see front matter © 2012 Elsevier B.V. All rights reserved.
http://dx.doi.org/10.1016/j.colsurfb.2012.04.007

The properties of the obtained Au–Pt_{NPs} were characterized by scanning electron microscopy (SEM), electrochemical impedance spectroscopy (EIS), and CV. Then amino groups modified probe ssDNA was immobilized on the Pty film via the affinity of amino groups to Au–Pt_{NPs} [28,29]. The immobilization and hybridization of DNA were carefully characterized with EIS. The DNA electrochemical sensor was used to the detection of the PEP gene fragment, which is an important promoter of phosphoenolpyruvate carboxylase gene in many genetically modified crops, with a label-free method adopting EIS.

2. Experimental

2.1. Apparatus and reagents

A CHI 660C electrochemical analyzer (Shanghai CH Instrument Company, Shanghai, China), which was in connection with a glassy carbon modified working electrode (Φ = 2 mm), a saturated calomel reference electrode (SCE) and a platinum wire auxiliary electrode, was used for the electrochemical measurement. Scanning electron microscopy (SEM) was carried out using a JSM-5900 machine (JEOL, Japan). The pH values of all solutions were measured by a model pHS-25 digital acidimeter (Shanghai Leici Factory, Shanghai, China). All solutions were prepared with Aquapro ultrapure water (Ever Young Enterprises Development Co., Ltd, Chongqing, China).

Tyramine, $HAuCl_4{\cdot}4H_2O$, and $H_2PtCl_6{\cdot}6H_2O$ were purchased from Sigma (St. Louis, MO, USA). Sodium dodecylsulfate (SDS) was purchased from Shanghai Reagent Company (Shanghai, China) and used as received. All the chemicals were of analytical grades and solutions were prepared with ultrapure water.

Materials for the detection of PEP gene sequence: 20-base probe DNA, 20-base complementary sequence of probe DNA (namely target DNA, cDNA), 1-base mismatched DNA, 2-base mismatched DNA and noncomplementary sequence (namely ncDNA) were synthesized by Beijing SBS Gene Technology Limited Company. Their base sequences were listed as below:

probe DNA: 5′-NH_2-CAG CAC CTA GGC ATA GGT TC-3′
cDNA: 5′-GAA CCT ATG CCT AGG TGC TG-3′
ncDNA: 5′-TGC GAT AAA GGA AAG GCT AT-3′
1-base mismatched DNA: 5′-GAA CCT **C**TG CCT AGG TGC TG-3′
2-base mismatched DNA: 5′-GAA CCT **C**TG CCT AGG TG**G** TG-3′

All oligonucleotides stock solutions of 20-base oligomers (1.0 μM) were prepared using Tris–HCl solution (5.0 mM Tris–HCl, 50.0 mM NaCl, pH 7.0), which were stored at 4° C. More diluted solutions were obtained via diluting aliquot of the stock solution with ultrapure water prior to use. The hybridization solution was diluted with 2 × SSC, which consists of 0.30 M NaCl and 30.0 mM sodium citrate tribasic dihydrate ($C_6H_5Na_3O_7{\cdot}2H_2O$).

2.2. Fabrication of DNA electrochemical biosensor

For the electrochemical experiments, the GCE surface was freshly polished prior to each experiment with 1, 0.3, and 0.05 μm α-Al_2O_3 paste, respectively, and sonicated for 3 min with ultrapure water and ethanol, respectively.

The polytyramine film modified GCE (Pty/GCE) was obtained by dipping the pretreated GCE in an unstirred methanol solution containing 0.3 M NaOH and 0.1 M tyramine and then cycling in the potential range from 0 V to +1.5 V at a scan rate of 50 mV/s for 16 cycles [22]. The Pty-modified electrode was carefully rinsed with ultrapure water to remove the untreated monomers. Then Au–Pt_{NPs} were electrodeposited to Pty film through potentiostatic method (PSA) at −0.2 V in 0.2 M Na_2SO_4 solution containing 1 mM $HAuCl_4$ and 1 mM H_2PtCl_6 for 1500 s [15]. After the electrodeposition of Au–Pt_{NPs}, the modified electrode was gently washed with ultrapure and air-dried at room temperature.

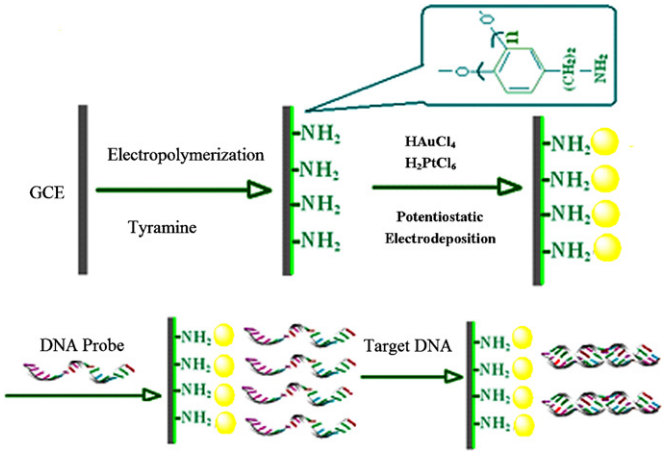

Fig. 1. Schematic representation of this DNA electrochemical biosensor.

To immobilize the probe DNA onto the surface of the modified electrode, the electrode should be immersed in 1.5 mL Tris–HCl buffer (pH 7.0) solution containing 1.0 μM probe DNA for 2.0 h at room temperature, followed by washing the electrode with 0.2% SDS solution for 5 min and then rinsing it with ultrapure water. The SDS could remove the unimmobilized ssDNA. Thus, the probe captured electrode (ssDNA/Au–Pt_{NPs}/Pty/GCE) was ready for use. Hybridization reaction was conducted by immersing the ssDNA/Au–Pt_{NPs}/Pty/GCE into a stirred hybridization solution containing 1.0 μM target DNA and keeping the working potential at +0.5 V for 500 s. Then the electrode was washed with 0.5% SDS for 5 min to remove the unhybridized DNA and this hybridization modified electrode was denoted as dsDNA/Au–Pt_{NPs}/Pty/GCE. The schematic representation of this DNA electrochemical biosensor is shown in Fig. 1.

2.3. Electrochemical measurements

All electrochemical measurements were carried out in a conventional three-electrode cell using CHI 660C electrochemical analyzer. The following parameters were employed for CV and DPV, respectively: CV: scan rate 100 mV/s; DPV: pulse amplitude 50 mV, pulse width 60 ms, pulse period 0.2 s. Supporting electrolyte solution of CV and DPV was 5.0 mM $K_3[Fe(CN)_6]$ and 5.0 mM $K_4[Fe(CN)_6]$ (1:1) solution containing 0.1 M KCl.

The EIS measurements were performed from 10^5 Hz to 0.1 Hz with 5 mV amplitude. The applied potential was 172 mV vs. SCE (formal potential of the redox probe $[Fe(CN)_6]^{3-/4-}$).

The reported result for every electrode in this paper was the mean value of three parallel measurements.

3. Results and discussion

3.1. SEM characterization of the composite modified electrodes

The surface morphology of the as-prepared Au–Pt nanoparticle film was characterized by SEM. Fig. 2 shows the typical SEM images of the as-prepared Au–Pt_{NPs} at different magnifications. Low-magnification SEM image (Fig. 2 left) reveals that the Au–Pt particles located at the polymer membrane were mono-dispersed with different sizes ranged from 50 nm to 1 μm irregularly. Au–Pt particles presents cauliflower-like shape, indicating that they were

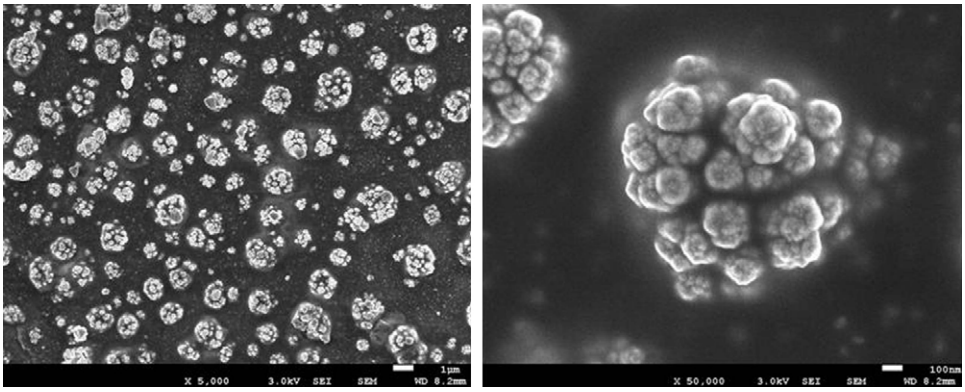

Fig. 2. The typical SEM images of Au–Pt_{NPs} at different magnifications (left 5000×, right 50,000×).

actually aggregate of nanoparticles as can be seen in the high-magnification image (Fig. 2 right).

3.2. Electrochemical characterization of the composite modified electrodes

The modified processes of different type of electrodes were monitored by CV in 5.0 mM $[Fe(CN)]^{3-/4-}$ solution containing 0.1 M KCl, as shown in Fig. 3. A pair of well-defined redox peaks could be observed at the bare GCE (Fig. 3 curve a). After the electrode was modified with polytyramine, the peak currents decreased evidently (Fig. 3 curve b) compared with that at the bare electrode, which could be attributed to the poor conductivity of non-conducting polytyramine [22]. For comparison, the sole Pt nanoparticles (Pt_{NPs}), sole Au nanoparticles (Au_{NPs}) and Au–Pt_{NPs} modifications on the Pty/GCE are shown in Fig. 3c–e, respectively. The values of the peak currents got larger and larger in above sequence, which demonstrated the active surface area of Au–Pt_{NPs} modified electrode was larger than those of the other four electrodes. This phenomenon should be ascribed to the excellent conductive properties of Au–Pt_{NPs} and the synergistic effects of Au–Pt_{NPs} and Pty.

3.3. Optimization of Au–Pt_{NPs} electrodeposition

The electrodeposition time of Au–Pt_{NPs} on the Pty/GCE was evaluated according to the DPV reductive peak current (I_P) of 5.0 mM $[Fe(CN)_6]^{3-/4-}$ solution containing 0.1 M KCl at Au–Pt_{NPs}/Pty/GCE, where electrodeposition was kept at −0.2 V by constant potential

Table 1
The relationship between the electrodeposition potential of Au–Pt_{NPs} on the Pty/GCE and the DPV reduction peak current at the Au–Pt_{NPs}/Pty/GCE. Supporting electrolyte solution is 5.0 mM $K_4[Fe(CN)_6]$ and 5.0 mM $K_3[Fe(CN)_6]$ containing 0.1 M KCl.

E (V)	0.0	−0.1	−0.2	−0.3	−0.4
I_p ($\times 10^{-4}$ A)	1.478	2.174	2.812	1.698	0.721

mode with varied electrodeposition times. The I_P increased gradually with the increase of the electrodeposition time and reached a maximum at 1500 s (shown in Fig. 4). After that, the I_P decreased slightly, which could be ascribed to that prolongation of the electrodeposition time led to the coagulation of the Au–Pt_{NPs}. Therefore, 1500 s was selected in our experiments.

Au–Pt_{NPs}/Pty/GCE electrodes were prepared in 0.2 M Na_2SO_4 solution containing 1 mM $HAuCl_4$ and 1 mM H_2PtCl_6 under different potentials such as 0 V, −0.1 V, −0.2 V, −0.3 V and −0.4 V for 1500 s. The above electrodes were also tested via DPV in 5.0 mM $[Fe(CN)_6]^{3-/4-}$ solution containing 0.1 M KCl, respectively. Accompanied by the negative shifts of the electrodeposition potential, the magnitude of the $[Fe(CN)_6]^{3-/4-}$ signal increased continually. The reduction peak current (I_p) reached the maximum when the Au–Pt_{NPs} were deposited under −0.2 V. When the electrodeposition potential was further shifted negatively, the I_p decreased obviously, indicating that the electric conductivity was weakened for less Au–Pt_{NPs} deposition on the surface of the electrode. Therefore, −0.2 V was selected as the potential for the Au–Pt_{NPs} film electrodeposition. The results are illustrated in Table 1.

The ratio of $HAuCl_4$ to H_2PtCl_4 had a pronounced effect on the electrochemical performance of the alloy nanoparticles composite film modified electrode [15]. Different volume ratios of

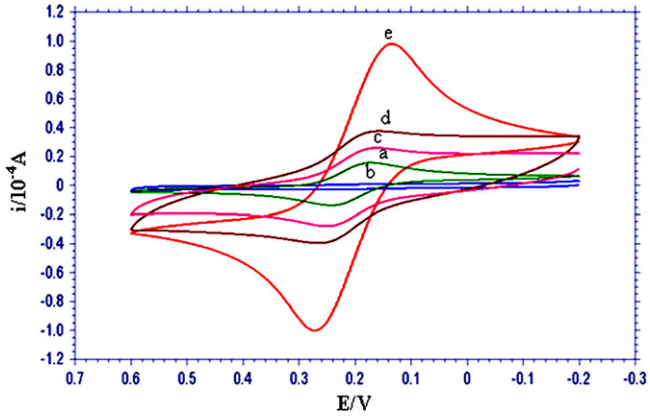

Fig. 3. Cyclic voltammograms of 5.0 mM $[Fe(CN)_6]^{3-/4-}$ recorded at (a) GCE, (b) Pty/GCE, (c) Pt_{NPs}/Pty/GCE, (d) Au_{NPs}/Pty/GCE, and (e) Au–Pt_{NPs}/Pty/GCE in 0.1 M KCl. Scan rate: 100 mV/s.

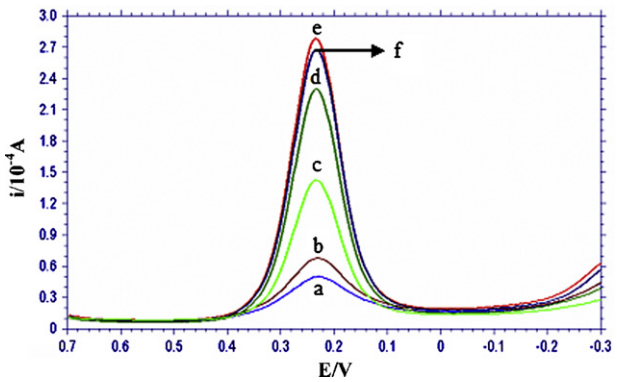

Fig. 4. Effect of the deposition time on the DPV reductive peak current of $[Fe(CN)_6]^{3-/4-}$ at Au–Pt_{NPs}/Pty/GCE: (a) 300 s, (b) 600 s, (c) 900 s, (d) 1200 s, (e) 1500 s, and (f) 1800 s. Supporting electrolyte solution is 5.0 mM $K_4[Fe(CN)_6]/K_3[Fe(CN)_6]$ containing 0.1 M KCl.

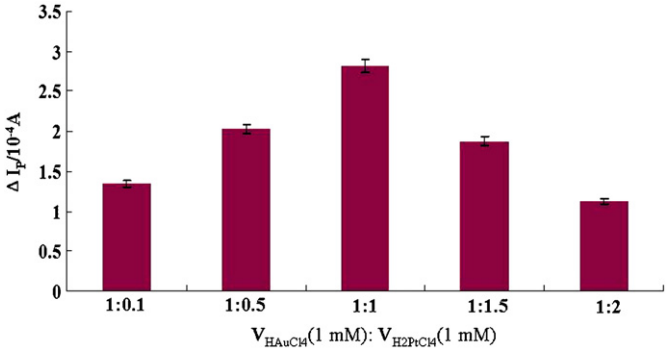

Fig. 5. Effect of the ratio of $V_{HAuCl_4(1\ mM)}$: $V_{H_2PtCl_4(1\ mM)}$ in composite on DPV reductive peak current difference (ΔI_P) of 5.0 mM $[Fe(CN)_6]^{3-/4-}$ in 0.1 M KCl between Au–Pt_{NPs}/Pty/GCE and Pty/GCE. (Each point was the mean of three measurements, and the error bars correspond to the standard deviation.)

1 mM $HAuCl_4$ to 1 mM H_2PtCl_4, such as 1:0.1, 1:0.5, 1:1, 1:1.5 and 1:2.0, were selected to seek the best ratio. The effect of the volume ratio of $HAuCl_4$ to H_2PtCl_4 (V_{HAuCl_4} : $V_{H_2PtCl_4}$) on the DPV reductive peak current difference (ΔI_P) of $[Fe(CN)_6]^{3-/4-}$ between Au–Pt_{NPs}/Pty/GCE and Pty/GCE is shown in Fig. 5. (Each point was the mean of three measurements, and the error bars correspond to the standard deviation.) The histogram shows that the ΔI_P increased with the decrease of V_{HAuCl_4} : $V_{H_2PtCl_4}$ and reached a maximum value at V_{HAuCl_4} : $V_{H_2PtCl_4}$ of 1:1. Then, the ΔI_P decreased with the further decrease of the $HAuCl_4$ proportion. So, the optimal ratio of V_{HAuCl_4} : $V_{H_2PtCl_4}$ was selected as 1:1.

3.4. Electrochemical impedimetric behavior of $[Fe(CN)_6]^{3-/4-}$ at DNA/Au–Pt_{NPs}/Pty/GCE

Nyquist diagrams of $[Fe(CN)_6]^{3-/4-}$ at different modified electrodes are illustrated in Fig. 6. The curve a was the Nyquist diagram recorded at bare GCE, and the high frequency section of the curve showed an arc with a given diameter ($R_{et} = 0.635 \times 10^3\ \Omega$, *Note*: the surface electron transfer resistance value, R_{et}, in the spectrum corresponds to the diameter of the semicircle). The curve b was the Nyquist diagram recorded at the Pty/GCE. Compared with curve a, the R_{et} of curve b greatly increased. The reason was ascribed to the nonconductive polytyramine film. When Au–Pt_{NPs} were electrodeposited on the Pty/GCE, we found an arc with a small diameter at high frequency section of the Nyquist diagram ($R_{et} = 0.483 \times 10^3\ \Omega$, curve c), which could be attributed to the Au–Pt_{NPs} enhancing the conductivity and enlarging the surface area of the electrode [6]. When ssDNA probe was immobilized on the Au–Pt_{NPs}/Pty/GCE, the

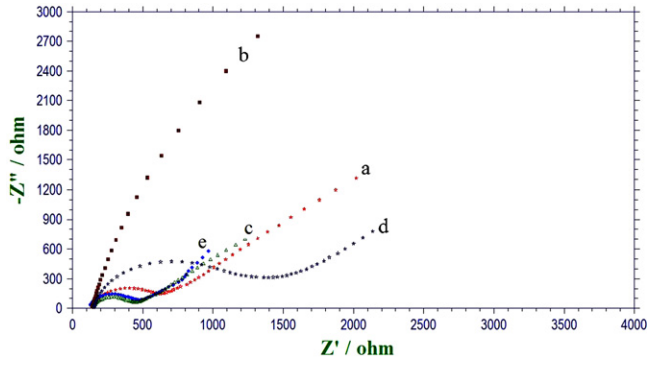

Fig. 6. Nyquist plots recorded at (a) bare GCE, (b) Pty/GCE, (c) Au–Pt_{NPs}/Pty/GCE, (d) ssDNA/Au–Pt_{NPs}/Pty/GCE, and (e) Au–Pt_{NPs}/Pty/GCE dipped to Tris–HCl buffer (pH 7.0) solution just without DNA existing. Supporting electrolyte solution is 5.0 mM $K_4[Fe(CN)_6]/K_3[Fe(CN)_6]$ containing 0.1 M KCl.

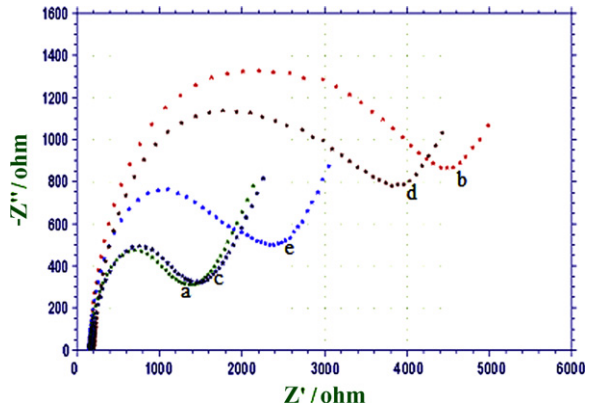

Fig. 7. Nyquist diagrams recorded at (a) ssDNA/Au–Pt_{NPs}/Pty/GCE, (b) dsDNA/Au–Pt_{NPs}/Pty/GCE (hybridized with cDNA), (c) the electrode hybridized with ncDNA, (d) the electrode hybridized with 1-base mismatched DNA, and (e) the electrode hybridized with 2-base mismatched DNA. Conditions are the same as in Fig. 6.

R_{et} of the electrode increased obviously ($R_{et} = 1.263 \times 10^3\ \Omega$, curve d). The electronegative phosphate skeletons of DNA prevented $[Fe(CN)_6]^{3-/4-}$ from reaching the electrode surface, thus enlarging the R_{et} of the electrode. The change from EIS during the modification processes was a strong evidence for ssDNA having been immobilized on the electrode surface [7]. For comparison, Nyquist plot of controlled Au–Pt_{NPs}/Pty/GCE, which dipped to Tris–HCl buffer (pH 7.0) solution just without DNA existing for 2.0 h at room temperature, was also recorded as shown in Fig. 6 (curve e). It could be seen that the shape and R_{et} varied weakly, and so the enhancement of R_{et} between curve c and curve d should be ascribed to the immobilization of ssDNA.

3.5. Optimization of DNA immobilization and hybridization conditions

The adsorption time of probe DNA was also optimized. The R_{et} values of the ssDNA/Au–Pt_{NPs}/Pty/GCE and Au–Pt_{NPs}/Pty/GCE for the probe DNA adsorption times of 0.5, 1.0, 1.5, 2.0 and 2.5 h, respectively, were recorded. With the increase of adsorption time, the differences of the R_{et} between ssDNA/Au–Pt_{NPs}/Pty/GCE and Au–Pt_{NPs}/Pty/GCE rose gradually at first (up to 2.0 h) and then reached a constant level. Therefore, an adsorption time of 2.0 h was used in our experiments.

The hybridization potential and time have important influence on hybridization efficiency and speed. The probe DNA hybridized with cDNA at different constant potentials, such as 0.3, 0.4, 0.5, 0.6 and 0.7 V, the related EIS was recorded. With the positively shift of the hybridization potential from 0.3 V to 0.5 V, the ΔR_{et} ($\Delta R_{et} = R_{dsDNA} - R_{ssDNA}$) value increased with the increase of the hybridization potential. With further increase of the hybridization potential, ΔR_{et} reached a constant level. Moreover, the probe DNA hybridized with cDNA at 0.5 V from 100 to 800 s. The ΔR_{et} value increased with the increase of the time from 100 to 500 s. With further increase of the hybridization time, the ΔR_{et} tended to stable. The optimal hybridization of the probe DNA was performed at 0.5 V for 500 s.

3.6. Detection of sequence-specific DNA of PEP gene

The selectivity of DNA hybridization could be judged by the hybridization of the probe DNA with different DNA sequences. As shown in Fig. 7, the curve a was the Nyquist diagram of $[Fe(CN)_6]^{3-/4-}$ at the probe DNA modified electrode, which was the same as curve d in Fig. 6. After hybridization of the probe DNA

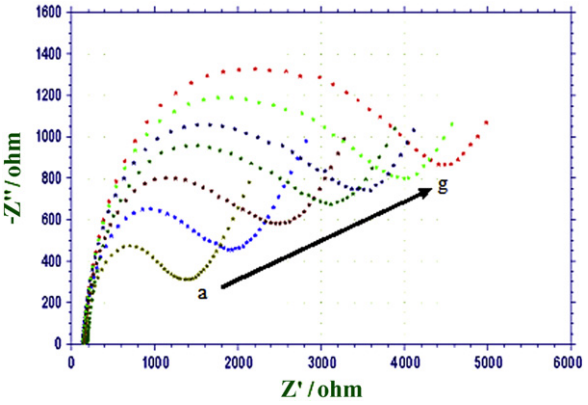

Fig. 8. Nyquist diagrams recorded at ssDNA/Au–Pt_{NPs}/Pty/GCE and after hybridization reaction with its complementary PEP gene sequence of different concentrations (M): (a) 0, (b) 1×10^{-12}, (c) 1×10^{-11}, (d) 1.0×10^{-10}, (e) 1×10^{-9}, (f) 1×10^{-8}, and (g) 1×10^{-7}. Conditions are the same as in Fig. 6.

with the complementary DNA under the optimal experimental conditions, the Nyquist diagram of $[Fe(CN)_6]^{3-/4-}$ was shown as the curve b, where the R_{et} value rose obviously. When the noncomplementary sequence was hybridized with the probe DNA (curve c), the R_{et} value varied little as compared with the probe DNA modified electrode. The 1-base mismatched sequence (curve d) and the 2-base mismatched sequence (curve e) could also be recognized via comparing the change of the R_{et} value. The results demonstrated that this DNA biosensor displayed a high selectivity for the hybridization detection.

The ΔR_{et} value between before and after hybridization was used to be the measurement signal to determine the sequence-specific related to the PEP gene fragment. The dynamic determination range was from 1.0×10^{-12} M to 1.0×10^{-7} M with the regression equation ΔR_{et} (Ω) = 500.49 log C + 6664.4 and the regression coefficient γ = 0.9986 (shown as in Fig. 8). The detection limit was 3.6×10^{-13} M using 3σ, where σ was the standard deviation of 11 parallel measurements of the blank solution. The result demonstrated that the sensitivity of this impedance-based DNA sensor was good enough for the PEP gene sequence detection.

3.7. The reproducibility and regeneration of the biosensor

To characterize the reproducibility of the electrode, five parallel-made DNA sensors were used to detect 1.0×10^{-10} M target DNA. The results of five dsDNA/Au–Pt_{NPs}/Pty/GCEs prepared independently under the same conditions showed a relative standard deviation (R.S.D.) of 5.16%, showing the good reproducibility of the electrochemical DNA biosensor.

The regeneration capability of this DNA sensor was also evaluated by denaturing the dsDNA (resulted from hybridization). The hybridized dsDNA was hot denatured by immersing the hybridized electrode into boiling water for 10 min, then cooled down rapidly with the ice salt bath, and followed by rinsing the electrode with ultrapure water. The Nyquist diagrams of 5.0 mM $[Fe(CN)_6]^{3-/4-}$ at the regenerated probe modified electrode and the hybridized dsDNA/Au–Pt_{NPs}/Pty/GCE were recorded. The results indicated that the two R_{et} values and ΔR_{et} value were almost the same as those obtained in the first experiment. Successive experiments showed that the DNA biosensor could be regenerated for 5 times without losing its sensitivity (83% of its initial signal), indicating the fine regeneration capability of the biosensor.

4. Conclusion

In summary, the Au–Pt_{NPs} were firstly immobilized to Pty film at the substrate electrode via electrodepositing method to prepare the Au–Pt_{NPs}/Pty/GCE, which served as a novel and efficient DNA immobilization matrix. The synergistic effect of Au–PtNPs and Pty could greatly improve the immobilization amount of the probe ssDNA on the electrode surface and further be benefit for DNA hybridization detection. On the other hand, the Au–Pt alloy nanoparticles could also improve electrochemical signal of the redox probe $[Fe(CN)_6]^{3-/4-}$, which is normally utilized as the indicator for the EIS detection of DNA layer. The DNA biosensor has been used to the detection of DNA sequence-specific of PEP gene with the electrochemical impedance spectroscopy owning high sensitivity and fine selectivity.

Acknowledgements

This work was supported by the National Natural Science Foundation of China (Nos. 20975057, 20805025), Doctoral Foundation of the Ministry of Education of China (No. 20113719130001) and Foundation of Qingdao City (No. 09-1-3-25-jch).

References

[1] C. James, http://www.isaaa.org/resources/publications/briefs/37/executivesummary/default.html.
[2] Y. Takahashi, T. Tojo, S. Nagahora, K. Yamazaki, J. Agric. Food Chem. 55 (2007) 2923–2929.
[3] J.E.N. Dolatabadi, O. Mashinchian, B. Ayoubi, A.A. Jamali, A. Mobed, D. Losic, Y. Omidi, M. Guardia, Trends Anal. Chem. 30 (2011) 459–472.
[4] E.G. Hvastkovs, D.A. Buttry, Analyst 135 (2010) 1817–1829.
[5] M. Du, T. Yang, K. Jiao, J. Mater. Chem. 20 (2010) 9253–9260.
[6] W. Zhang, T. Yang, X. Li, D.B. Wang, K. Jiao, Biosens. Bioelectron. 25 (2009) 428–434.
[7] T. Yang, N. Zhou, Y.C. Zhang, W. Zhang, K. Jiao, G.C Li, Biosens. Bioelectron. 24 (2009) 2165–2170.
[8] W. Zhang, T. Yang, X.M. Zhuang, Z.Y. Guo, K. Jiao, Biosens. Bioelectron. 24 (2009) 2417–2422.
[9] F. Xiao, F.Q. Zhao, Y.F. Zhang, G.P. Guo, B.Z Zeng, J. Phys. Chem. C 113 (2009) 849–855.
[10] S. Zhang, Y.Y. Shao, H.G. Liao, J. Liu, I.A. Aksay, G.P. Yin, Y.H. Lin, Chem. Mater. 23 (2011) 1079–1081.
[11] Z.M. Peng, H.J. You, H. Yang, Adv. Funct. Mater. 20 (2010) 3734–3741.
[12] S. Zhou, K. Mcllwrath, G. Jackson, B. Eichhorn, J. Am. Chem. Soc. 128 (2006) 1780–1781.
[13] J. Luo, P.N. Njoki, Y. Lin, D. Mott, L.Y. Wang, C.J. Zhong, Langmuir 22 (2006) 2892–2898.
[14] F. Xiao, Z.R. Mo, F.Q. Zhao, B.Z Zeng, Electrochem. Commun. 10 (2008) 1740–1743.
[15] L. Qian, X. Yang, J. Phys. Chem. B 110 (2006) 16672–16678.
[16] H. Lang, S. Maldonado, K.J. Stevenson, B.D. Chandler, J. Am. Chem. Soc. 126 (2004) 12949–12956.
[17] S. Cosnier, M. Holzinger, Chem. Soc. Rev. 40 (2011) 2146–2156.
[18] Y.W. Hu, T. Yang, X.X. Wang, K. Jiao, Chem. Eur. J. 16 (2010) 1992–1999.
[19] T. Yang, Y.W. Hu, W.J. Li, K. Jiao, Colloids Surf. B 83 (2011) 179–182.
[20] Y.Q. Miao, J.R. Chen, Y. Hu, Anal. Biochem. 339 (2005) 41–45.
[21] S.A. Miscoria, G.D. Barrera, G.A. Rivas, Sens. Actuators B: Chem. 115 (2006) 205–211.
[22] Z.S. Wu, J.S. Li, T. Deng, M.H. Luo, G.L. Shen, R.Q. Yu, Anal. Biochem. 337 (2005) 308–315.
[23] M. Situmorang, J.J. Gooding, D.B. Hibbert, Anal. Chim. Acta 394 (1999) 211–223.
[24] A.G. Mantzila, V. Maipa, M.I. Prodromidis, Anal. Chem. 80 (2008) 1169–1175.
[25] D.W. Hatchett, M. Josowicz, Chem. Rev. 108 (2008) 746–769.
[26] Y.C. Fu, P.H. Li, Q.J. Xie, X.H. Xu, L.H. Lei, C. Chen, C. Zou, W.F. Deng, S.Z. Yao, Adv. Funct. Mater. 19 (2009) 1784–1791.
[27] F.N. Crespilhoa, R.M. Iost, S.A. Travainc, O.N. Oliveira Jr., V. Zucolottob, Biosens. Bioelectron. 24 (2009) 3073–3077.
[28] H. Cai, C. Xu, P.G. He, Y.Z. Fang, J. Electroanal. Chem. 510 (2001) 78–85.
[29] X.X. Wang, T. Yang, X. Li, K. Jiao, Biosens. Bioelectron. 26 (2011) 2953–2959.